Arabian Journal of Chemistry (2022) **15**, 103677

King Saud University

Arabian Journal of Chemistry

www.ksu.edu.sa
www.sciencedirect.com

ORIGINAL ARTICLE

In vitro cytotoxicity against K562 tumor cell line, antibacterial, antioxidant, antifungal and catalytic activities of biosynthesized silver nanoparticles using *Sophora pachycarpa* extract

Zahra Kiani [a,1], Hamed Aramjoo [b,1], Elham Chamani [c], Mahin Siami-Aliabad [a,c], Sobhan Mortazavi-Derazkola [d,*]

[a] *Department of Pharmacology, Birjand University of Medical Sciences, Birjand, Iran*
[b] *Student Research Committee, Birjand University of Medical Sciences, Birjand, Iran*
[c] *Department of Clinical Biochemistry, Faculty of Medicine, Birjand University of Medical Sciences, Birjand, Iran*
[d] *Medical Toxicology and Drug Abuse Research Center (MTDRC), Birjand University of Medical Sciences, Birjand, Iran*

Received 23 September 2021; accepted 29 December 2021
Available online 4 January 2022

KEYWORDS

Green synthesis;
Sophora pachycarpa;
Nanoparticle;
Anti-cancer;
Photocatalytic degradation

Abstract In the present study, we demonstrate the green synthesis of silver nanoparticles using *Sophora pachycarpa* extract (*S. pachycarpa; SPE*) as capping, reducing, and stabilizing agents. The biosynthesized silver nanoparticles (*SPE*-AgNPs) were tested for catalytic, antibacterial, antifungal, antioxidant, and anti-cancer activities. The affecting parameters (the concentration of silver nitrate, the temperature of the reaction, and time of reaction) on the synthesis process were optimized. The biosynthesized *SPE*-AgNPs were studied by X-Ray diffraction (XRD), transmission electron microscopy (TEM), field emission scanning electron microscopy (FESEM), dynamic light scattering (DLS), energy-dispersive X-ray spectroscopy (EDS) and Fourier-transform infrared spectroscopy (FT-IR). The FESEM and TEM results revealed spherical and oval-like morphology with sizes ranging from 30 to 40 nm. Photocatalytic performance experiments of *SPE*-AgNPs were determined by the rapid degradation of the eriochrome black T (EBT) and methylene blue (MB) under sunlight and UV irradiations. The results showed that *SPE*-AgNPs degraded more than 90% and 80% of both dyes under UV and sunlight irradiations, respectively. In addition, the *SPE*-AgNPs exhibited good antibacterial and antifungal properties against *S. aureus*, *S. epidermidis*, *P. aeruginosa*, *E. coli*, *K. pneumoniae*, *E. faecalis*, and *C. albicans* with MIC values of 6.25, 6.25,

* Corresponding author.
E-mail addresses: S.mortazavi23@yahoo.com, Sobhan.mortazavi@bums.ac.ir (S. Mortazavi-Derazkola).
[1] ***These authors contributed equally to this work.***

Peer review under responsibility of King Saud University.

Production and hosting by Elsevier

https://doi.org/10.1016/j.arabjc.2021.103677

0.78, 0.39, 0.78, 1.56 and 0.78 μg/ml. The green synthesized *SPE*-AgNPs were found to inhibit the activity of DPPH free radicals efficiently. Eventually, the *SPE*-AgNPs exhibited significant in vitro cytotoxicity against K562 tumor cell line (IC50 = 19.5 μg/ml). All these studies indicated that AgNPs synthesized using *S. pachycarpa* extract have applications in the environmental and biomedical fields.

1. Introduction

Nanotechnology is an applied science with a wide range of applications in pharmaceutical science (Ardestani et al., 2020; Ghoreishi et al., 2017; Mohammadi-Aghdam et al., 2018), drug design (Yoo et al., 2015), biology (Chandra et al., 2020; Mohammadzadeh et al., 2019; Shirzadi-Ahodashti et al., 2020b), medicine (Guo et al., 2021; Mohammadzadeh et al., 2017), environment (Ahmadi et al., 2020b; Ebrahimzadeh et al., 2019; Ebrahimzadeh et al., 2020b), etc. Nanoparticles with sizes of 1–100 nm and various shapes have unprecedented chemical, physical and optical properties. Among metal nanoparticles, silver is one of the most important and widely used ones in the pharmaceutical, environmental and cosmetic industries (Rafique et al., 2017). Silver nanoparticles offer unique physical and chemical properties such as high electrical and thermal conductivity, suitable size, chemical stability, catalytic activity, and biological properties such as antimicrobial, antioxidant, anticancer effects (Beyene et al., 2017; Naghizadeh et al., 2021). Fouda *et al.* found that silver nanoparticles can be used to produce bioactive compounds that are applicable in biomedicine with significant antioxidant and antimicrobial properties (Fouda et al., 2020).

Various methods such as chemical reduction, lithography, electrochemistry, lasers, and microwaves are used to synthesize metal nanoparticles (Iravani et al., 2014). One of the disadvantages of chemical approaches is that they remain undecomposed and eventually cause pollution. In addition, the use of high pressure and high temperature during the synthesis of nanoparticles, even in low quantities, consumes lots of resources (Jorge de Souza et al., 2019). To solve this problem, the researchers used a wide range of environmentally friendly solvents. One of the goals of green chemistry is to use environmentally friendly reactants (Rao and Trivedi, 2006). This approach has advantages such as ease of use, biosafety and biocompatibility, lower costs, nontoxicity, and the production of high purity nanoparticles. Garibo *et al.* showed in 2020 that nanoparticles synthesized through the green synthesis, while less cytotoxic, have more antimicrobial effects than chemically synthesized silver nanoparticles (Garibo et al., 2020).

The rapid growth of industries such as textiles, dyes, and large amounts of plastic waste that end up in water, lead to serious environmental pollution. Dye contaminants, being one of the most essential contaminations, affects the transparency of water and causes the abnormal color of water (Azeez et al., 2018). Various methods, such as adsorption or coagulation, have been used to remove organic matter. One of the efficient methods of removing organic dyes developed over the last few decades is photocatalysts (Mekasuwandumrong et al., 2010; Shirzadi-Ahodashti et al., 2020a). Various studies have been carried out to date on the photocatalytic properties of silver nanoparticles. Kadam *et al.* introduced silver nanoparticles as an effective multifunctional tool for dye degradation (methylene blue) in industrial effluents and the detection of mercury-based contaminants (Kadam et al., 2020). Rajkumar *et al.* also reported that green silver nanoparticles synthesized with *Chlorella vulgaris* degraded 96.51% of methylene blue dye (100 ppm) within 3 h of incubation (Rajkumar et al., 2021). In previous research, the destruction of pollutants has not been significant. In this study, we obtained the high degradation efficiency of contaminants using biosynthesized nanoparticles.

Over the last five decades and the decline in the death rate from infectious diseases, cancer has become the leading cause of death in developed countries. The cancer cell line K562 is a myeloid blood leukemia cell that was first observed in a 53-year-old woman with chronic leukemia. It has about 1.5 times as many chromosomes as normal cells (Klein et al., 1976). In recent years, the effects of synthesized nanoparticles on different types of cancer cells were investigated (Ahmed et al., 2019; Anandan et al., 2019). Hashemi *et al.,* by studying the antitumor property of silver nanoparticles, found that these nanoparticles have potential therapeutic effects and could be valuable in the production of cancer drugs (Hashemi et al., 2020). Ahmadi *et al.* also assessed the cytotoxic effects of silver nanoparticles on K562 and MCF-7 cell lines (Ahmadi et al., 2020a).

Sophora is a perennial herb with 7–12 pairs of leaves, cream-colored flowers, and fruits of the genus Fabaceae, widespread in East and Southwest Asia, Greece and southern Russia. The biologically active compounds of this genus include quinolizidine alkaloids, flavonoids, and steroidal glucosides (Emami et al., 2007). The antimicrobial, sedative, antipyretic, analgesic, anti-inflammatory, and antitumor effects of quinolizidine alkaloids, and the antioxidant, antibacterial, anti-inflammatory, anticancer, and antiviral effects flavonoids have already been proven (Kumar and Pandey, 2013).

This study aimed to green synthesize silver nanoparticles using hydroalcoholic *Sophora pachycarpa* extract (*S. pachycarpa*) and use it as an antibacterial and antifungal agents against Gram-positive bacteria (*S. aureus, S. epidermidis,* and *E. faecalis*) and Gram-negative bacteria (*P. aeruginosa, E. coli,* and *K. pneumoniae*) and *C. albicans* as fungal. The potential anticancer effect of the synthesized nanoparticles on K562 cell line was also assessed through the MTT assay. In addition, the photocatalytic activity was investigated by the degradation of eriochrome black T and methylene blue dyes under UV and sunlight irradiations.

2. Materials and methods

2.1. Materials and characterization techniques

All chemical reagents were at least reagent grade. Silver nitrate ($AgNO_3$, 99.99%), sodium hydroxide (NaOH), and methanol solution were obtained from Sigma-Aldrich Company. All water used in the experiment was triply deionized water. The fresh parts of *S. pachycarpa* were collected from the Southern Khorasan province of Iran and washed with deionized water. Characterization of biosynthesized silver nanoparticles was determined by using various analytical techniques such as field emission scanning electron microscopy (FE-SEM; TESCAN BRNO-Mira3 LMU), Fourier transform infrared spectroscopy (FT-IR; PerkinElmer Spectrum Two^{TM} IR spectrometer; Model L160000U), UV-Visible spectroscopy (NanoDrop, BioTek model Epoch, USA), dynamic light scattering (DLS; NanoBrook 90Plus-Brookhaven Instruments, model 18051; USA; DLS), X-ray diffraction (Philips PW 1800 using Cu Kα radiation), transmission electron microscopy (TEM; Zeiss-EM10C-100 KV) and energy-dispersive X-ray spectroscopy (EDS).

2.2. Preparation of Sophora pachycarpa extract (SPE)

A herbarium specimen of *Sophora pachycarpa* was identified by a botanist and examined and approved by a specialist in the Herbarium of Birjand University of Medical Sciences in May 2020 in South Khorasan, Iran. The plant roots were pulverized by a grinder and the alcoholic extract was stirred by soaking the powder in a 1:10 solution of 80% methanol at room temperature for 24 h. The mixture was then filtered using a paper filter (Blue Ribbon, Grade 589, Germany), and its solvent was concentrated using a rotary evaporator (Heidolph, Germany), then was dried by a freeze dryer (FD-5005-BT, Dena Vacuum Industry, Iran), and powder was stored at −20 °C until use.

2.3. Biosynthesis of silver nanoparticles using SPE (SPE-AgNPs)

The *SPE* capped AgNPs (*SPE*-AgNPs) were synthesized using our previous protocol (Shirzadi-Ahodashti et al., 2021a). Typically, 0.3 g of *S. pachycarpa* extract was dissolved in 20 ml of distilled water, and the pH was raised to 12. The preparation of silver nanoparticles was observed by a color change from yellow to blood red according to the surface plasmon resonance (SPR). After that, the silver solution was further centrifuged and washed three times at room temperature. Finally, the purified AgNPs were stored for further study. Furthermore, a description of the samples prepared under different conditions is exhibited in Table. 1.

Table 1 Experimental detail for green synthesis of AgNPs using *S. pachycarpa* extract.

Sample no.	Ag concentration (mM)	Time (min)	Temperature (°C)	Figure of UV
1	5	30	25	Fig. 1a
2	10	30	25	Fig. 1a
3	15	30	25	Fig. 1a
4	20	30	25	Fig. 1a
5	40	30	25	Fig. 1a
6	40	5	25	Fig. 1b
7	40	15	25	Fig. 1b
8	40	60	25	Fig. 1b
9	40	90	25	Fig. 1b
10	40	60	60	Fig. 1c
11	40	60	85	Fig. 1c

2.4. Antibacterial and antifungal assay

Staphylococcus aureus (ATCC 16538; *S. aureus*), *Staphylococcus epidermidis* (ATCC 12228; *S. epidermidis*), *Pseudomonas aeruginosa* (ATCC 27853; *P. aeruginosa*), *Escherichia coli* (ATCC 25922; *E. coli*), *Klebsiella pneumoniae* (ATCC 9997; *K. pneumoniae*), *Enterococcus faecalis* (ATCC 15753; *E. faecalis*), and *Candida albicans* fungi (*C. albicans*), were obtained from the Pasteur Institute of Iran. To obtain pure colonies from the nutrient broth culture medium containing pathogenic bacteria, an isolated culture was performed on the nutrient and blood agar media to obtain a 0.5 McFarland solution (1.5×10^8 CFU/ml) from the colonies that appeared on the surface of the culture medium. *C. albicans* fungi colonies were used to make suspension after revitalization and purification in the Sabouraud dextrose agar medium. For minimum inhibitory concentration (MIC) experiment: 100 µl TSB (Tryptic Soy Broth) was added to the culture medium in each micro-well, and 100 µl of the nanoparticle solution produced was added to the first micro-well of each row and mixed. The MIC was considered as the lowest concentration of bacterial growth inhibitor (Riesenberg et al., 2016). In this study, ceftriaxone as an antibiotic and amphotericin B as an antifungal was used to compare the antibacterial and antifungal effects of the nanoparticles and the extract, respectively. In order to do determine the minimum bactericidal concentration (MBC), 10 µl of turbidity-free micro-wells (at MIC concentrations and above) was taken under completely sterile conditions and inoculated and cultured on a blood agar medium. After 24 h of incubation at 37 °C, the most minor dilution that killed 99.9% of the bacteria indicated the MBC. For the reliability of the result, the experiment was repeated three times and an average was calculated (Ebrahimzadeh et al., 2020a).

2.5. Antioxidant activity

To examine the antioxidant properties, we used Zantox Total Antioxidant Capacity (TAC) Assay Kit (Kavosh Arian Azma Co., Iran) based on DPPH (2,2-diphenyl-1-picrylhydrazyl) assay. In this standard method, 10 µl of *S. pachycarpa* extract samples, *SPE*-AgNPs (sample no. 11), control sample (available in the kit), distilled water (blank sample), and various standards (in concentrations of 62.5, 125, 250, 500, and 100 µM) were poured into micro-wells. Then 250 µl of the prepared DPPH solution was added to each of the micro-wells according to the kit protocol, and the plate was shaken for 30 s. Finally, samples were incubated in the dark at room temperature for 15 min and their absorption was measured at 517 nm using a spectrophotometer. The radical scavenging of DPPH was calculated as follow (Morabbi Najafabad and Jamei, 2014):

DPPH radical scavenging (%)

$$= [(A_0 - - A_1)/A_0] \times 100 \quad (1)$$

where A_0 is the absorbance of the DPPH solution, and A_1 is the absorbance of the sample.

2.6. MTT assay of antitumor properties of SPE-AgNPs

The K562 (Chronic Myeloid Leukemia) Cells were cultured in a complete RPMI 1640 medium containing 10% FBS and 1% Pen/Strep at 37 °C in a humidified atmosphere of 5% CO_2. The cytostatic effect of *SPE*-AgNPs on K562 cells was investigated by MTT methods. The Cells in exponential phase and the number of passage three were centrifuged, and plate was collected. Then, 20×10^3 cells/ml was added to each well of 96-well cell culture micro-plate in triplicate and treated with concentrations of 6.25, 12.5, 25, and 50 µg/ml of *SPE*-AgNPs. After 24 h of incubation (5% CO_2 and 37 °C), 20 µl of the MTT solution (5 mg MTT dissolved in 1 ml PBS) was added to each micro-well and further incubated for 3 h. 100 µl of DMSO solution was then added to each micro-well. After 10–15 min and upon dissolution of the formazone particles, the absorption was measured at a wavelength of 570 nm with an ELISA reader (Mosmann, 1983). The survival rate was calculated as follow:

Viability (%) = (sample absorption / control absorption) × 100 (2)

2.7. Photocatalytic activity

In order to investigate the photocatalytic degradation properties of eriochrome black T (as an anionic contaminant) and methylene blue (as a cationic contaminant), the synthesized *SPE*-AgNPs (sample no. 11; optimized sample) was applied to degrade the pollutants in a reactor under sunlight and UV irradiations. The photocatalytic experiment was performed by applying 5 ppm of methylene blue (main absorbance band at λ = 668 nm) and 10 ppm of eriochrome black T (main absorbance band at λ = 574 nm). 30 mg of *SPE*-AgNPs was added into 50 ml of each contaminants solution and stirred for 30 min without irradiation to reach the absorption equilibrium. Next, at the specified time intervals, 10 ml of suspension was withdrawn, centrifuged (6000 rpm and 10 min) to separate the photocatalyst, and determined by UV-Vis spectrophotometer. The contaminants degradation percentage was calculated as follow (Ghoreishi, 2017): D (%) = $(A_0\text{-}A_t)/A_0$ * 100 (3); where D is the photocatalytic efficiency (after t min), A_0 is the initial absorbance quantity of pollutants solution and A_t is the absorbance of anionic and cationic contaminants after irradiation (after t min).

3. Results and discussion

3.1. UV-Vis spectrographic analysis

The best formation of AgNPs (in terms of size and morphology) depends on some factors (such as concentration, temperature, and time). The surface plasmon resonance (SPR) of synthesized biogenic silver nanoparticles exhibited a peak centered about 420 nm related to the absorbance of AgNPs (Shirzadi-Ahodashti et al., 2021b). So, in this research, evaluation of various critical experimental parameters, including the

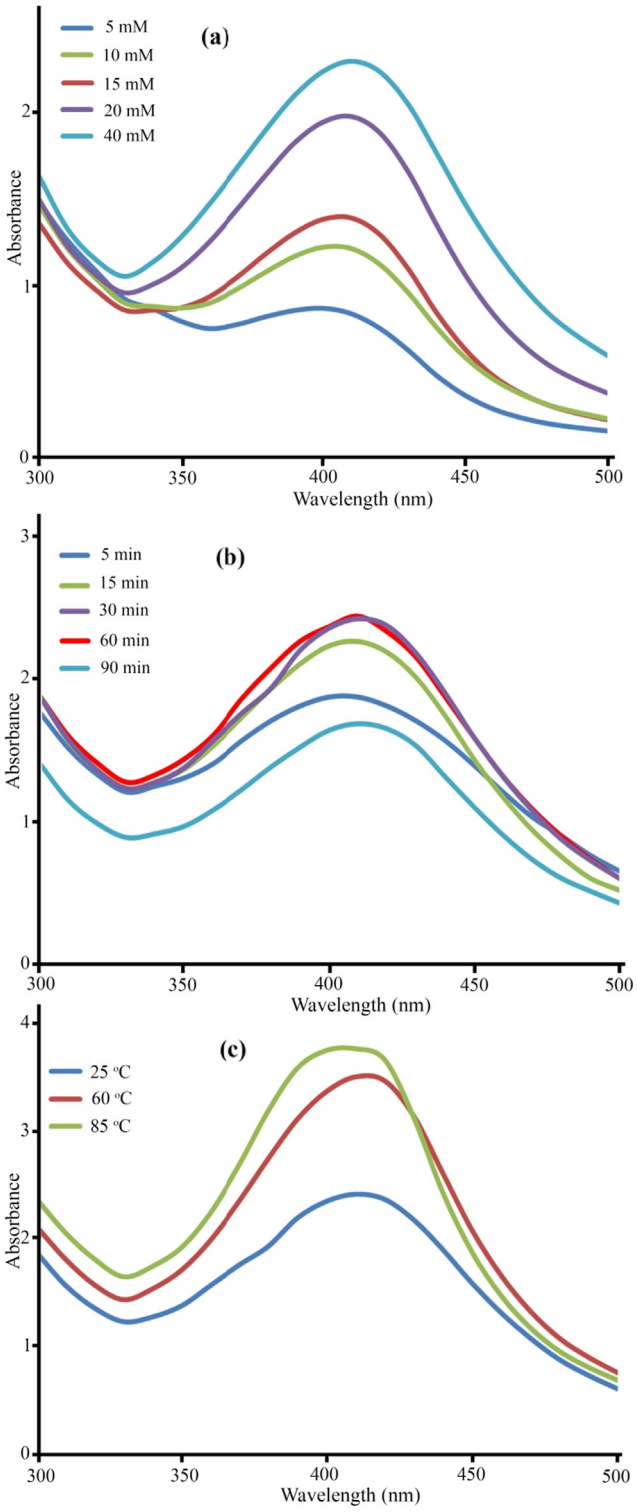

Fig. 1 UV-Vis absorption spectra of AgNPs at various conditions: (a) concentration of $AgNO_3$ (5, 10, 15, 20, and 40 mM), (b) time (5, 15, 30, 60, and 90 min) and (c) temperature (room tempt., 60, and 85 °C.).

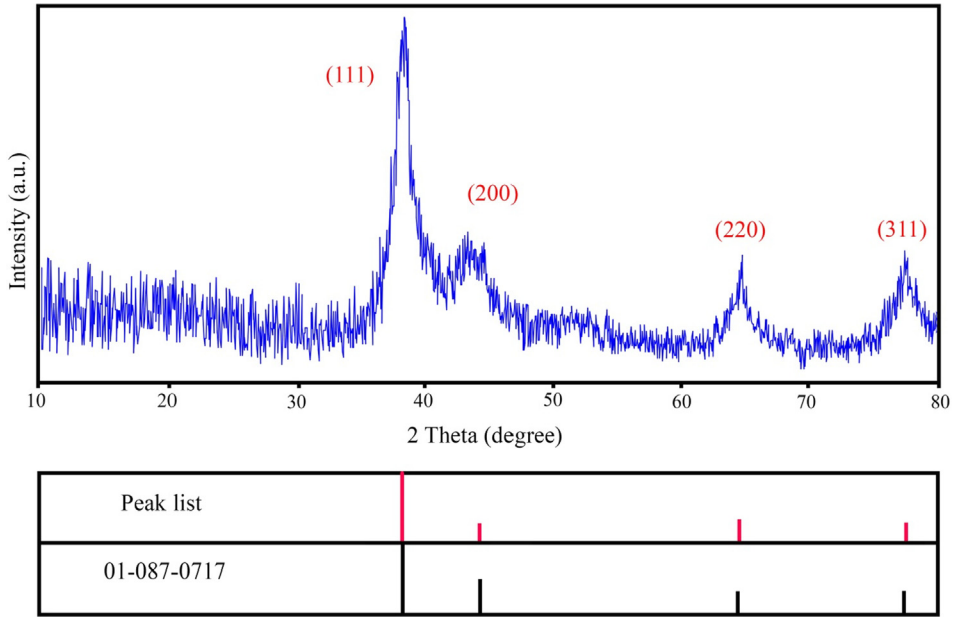

Fig. 2 XRD pattern of biosynthesized AgNPs using *S. pachycarpa* extract (40 mM, 60 min and 85 °C).

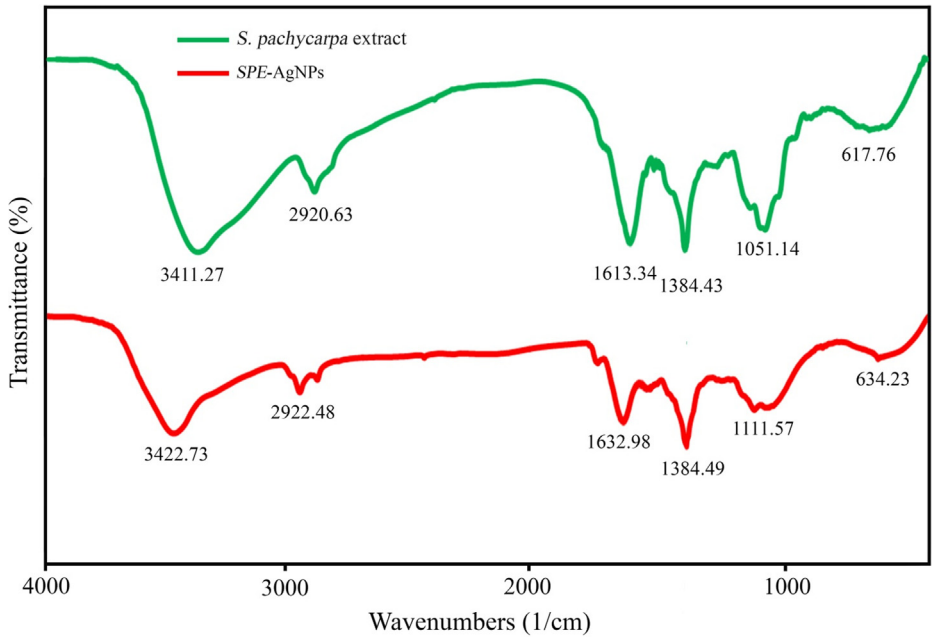

Fig. 3 FT-IR spectrum of the S. *pachycarpa* extract and *SPE*-AgNPs (40 mM, 60 min and 85 °C).

concentration of silver ion (5, 10, 15, 20, and 40 mM), reaction time (5, 15, 30, 60, and 90 min), and temperature (room temp., 60, and 85 °C) were studied. Each of these experimental parameters was confirmed by UV-Vis spectral study.

3.1.1. Effect of silver ion concentration

Fig. 1a shows the UV-Vis spectra of the AgNPs synthesized using 5 ml of *S. pachycarpa* extract in the presence of $AgNO_3$ concentrations varying from 5 mM to 40 mM. As can be seen, 40 mM concentration of silver nitrate with 5 ml of *S. pachycarpa* extract illustrates more absorbance than the other four concentrations (5, 10, 15, and 20 mM). Past research showed that increasing the $AgNO_3$ concentrations enhanced the absorption intensity implying the increase in the formation of nanoparticles (Hebeish et al., 2013). Therefore, the optimum value of the $AgNO_3$ concentration is 40 mM, which was applied for the next experiments.

3.1.2. Effect of contact time

Fig. 1b shows the UV-Vis spectra recorded at different reaction times. As can be seen, increasing the contact time increased the intensity of the SPR band (5–60 min). However, by increasing the reaction time from 60 to 90 min, there was a decrease in the intensity of the SPR band. This decrease is

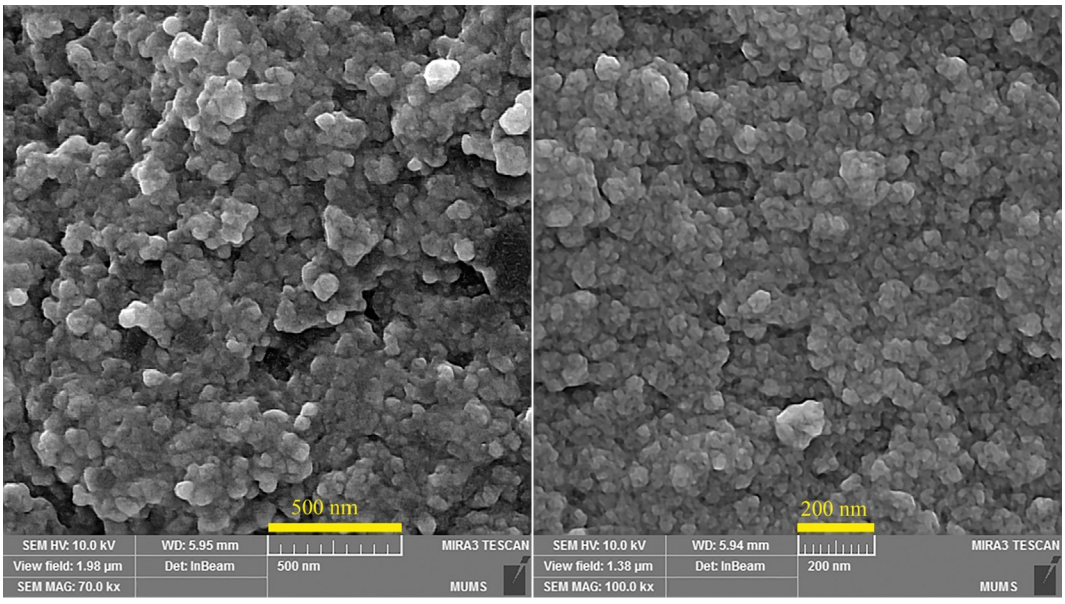

Fig. 4 FESEM images of the biosynthesized AgNPs using *S. pachycarpa* extract (40 mM, 60 min and 85 °C).

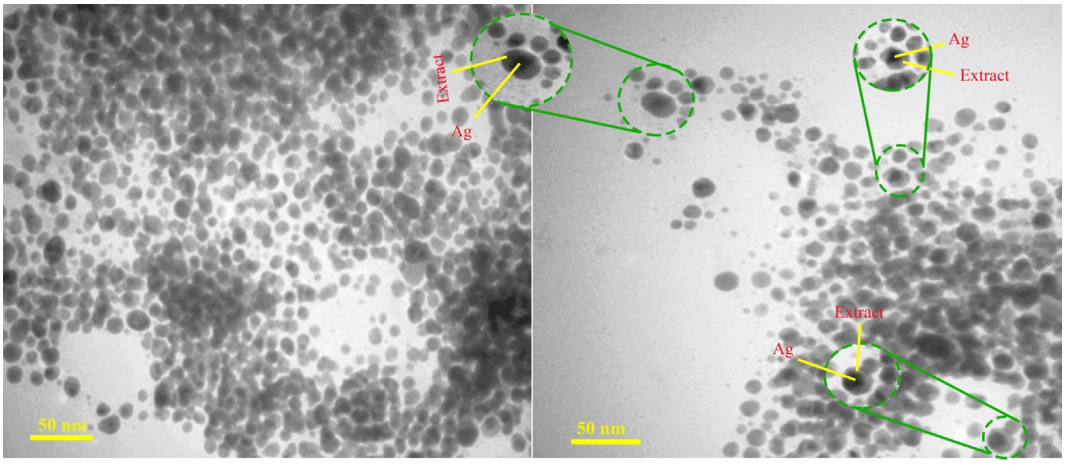

Fig. 5 TEM images of *SPE*-AgNPs (40 mM, 60 min and 85 °C).

related to the increased agglomeration of the obtained products. So, the optimal contact time to obtain silver nanoparticles of suitable size and morphology is 60 min.

3.1.3. Effect of temperature

The influence of the reaction temperature on the preparation of silver nanoparticles is exhibited in Fig. 1c. The UV results showed that with increasing temperature, the intensity of adsorption increased. Moreover, decreasing wavelength (blue shift) from 423 to 411 cm^{-1} can be observed with temperature increasing (from room temp. to 85 °C). From this reduction, it can be concluded that AgNPs with smaller sizes can be obtained at a higher temperature. So, the optimum value of the temperature is 85 °C.

3.2. X-ray diffraction

The crystallinity and nature of the synthesized silver particles using *S. pachycarpa* extract (under the best conditions) was evaluated by X-ray diffraction (XRD). The XRD pattern of AgNPs, which confirmed the crystalline nature of silver nanoparticles, was shown in Fig. 2. The four distinct diffraction peaks at 38.37°, 44.34°, 64.62°, and 77.59° in the range 10–80°, can be related to the (111), (200), (220), and (311) Bragg reflections from the fcc structure of nanoparticles (JSDS 01-087-0717). Moreover, no impurities were observed in XRD pattern that indicating that the crystal was a single phase. Our results were matched with the findings of Awwad *et al.* (Awwad et al., 2013). In addition, the grain size of biosynthesized metallic silver nanoparticles was determined using the Debye-Scherrer equation: $D = n\lambda/\beta\cos\theta$ (4). Where λ is the X-ray wavelength, D is the crystallite size, θ is the diffraction angle and β is full-width half maximum (FWHM). Based on the above equation, the size of the synthesized nanoparticles was determined about 32 nm.

3.3. Fourier transforms infrared (FTIR) analysis

The investigation of the functional groups in the silver ion (Ag^{+}) reduction using *S. pachycarpa* extract for the green syn-

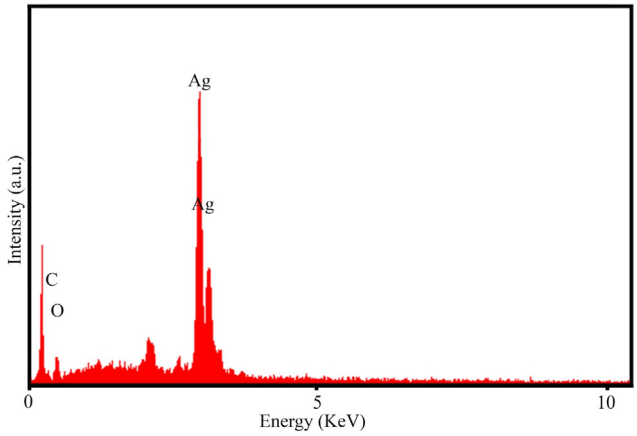

Fig. 6 EDS analysis representing the compositional analysis of *SPE*-AgNPs (40 mM, 60 min and 85 °C).

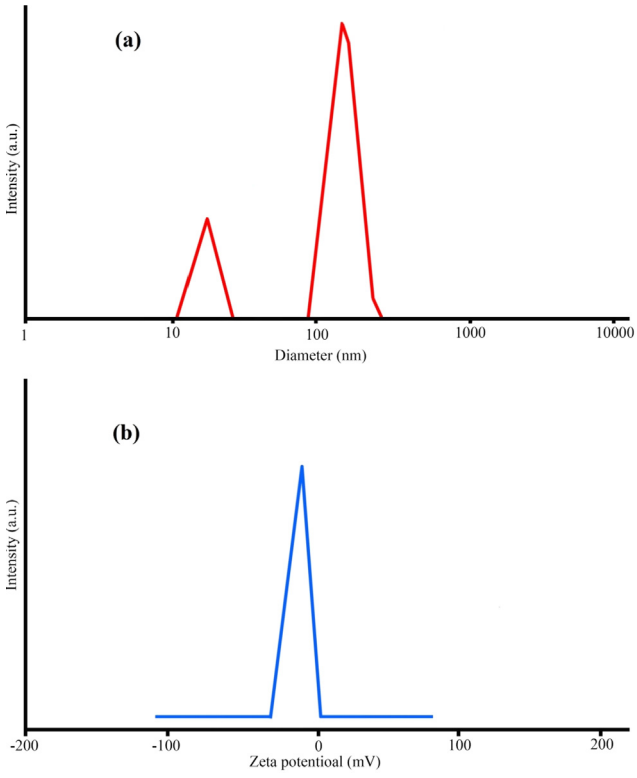

Fig. 7 (a) DLS and (b) zeta potential measurement of *SPE*-AgNPs (40 mM, 60 min and 85 °C).

thesis of AgNPs is shown in Fig. 3. The strong and broad absorption band at around 3400 cm^{-1} is related to the hydroxyl stretching band (O-H) of the phenolic compounds in the plant extract (Judith Vijaya et al., 2017). The band at approximately 2920 cm^{-1} can be related to methylene or methyl stretching vibration (C-H). The peaks at around 1600 and 1300 cm^{-1} corresponds to phenolic group and stretching aromatic ring (-C = C), respectively. So, water-soluble plant metabolites like quinones, flavonoids, and polyphenols were possibly responsible for reducing metal ions (Ag^{+}) into silver nanoparticles (Ag^{0}). As seen in the FTIR spectra of *SPE*-AgNPs, the absorption peaks of *SPE*-AgNPs were similar to the *S. pachycarpa* extract absorption peaks with a minor amount of displacement and intensity than absorption peaks of *S. pachycarpa* extract, which was consistent with the results of previous studies (Li et al., 2021).

3.4. FESEM, TEM, and EDX analysis

The size and morphology of biosynthesized silver nanoparticles were investigated by field emission scanning electron microscopy (FESEM) images with different magnifications. Fig. 4 shows the FESEM micrographs of as-synthesized silver nanoparticles in the presence of *S. pachycarpa* extract with different magnifications (*SPE*-AgNPs). The results showed that the produced nanoparticles are spherical-like, and agglomerated in some areas. This agglomeration confirms the presence of stabilizing and capping agents in the process of formation AgNPs. Furthermore, regular and uniform structures with sizes in the range of 30–40 nm are another characteristic of synthesized nanoparticles. Fig. 5 shows TEM images of the synthesized silver nanoparticles in the presence of *S. pachycarpa* extract (optimized sample; *SPE*-AgNPs). Uniform nanoparticles and suitable distribution extract on the surface of silver nanoparticles are illustrated in Fig. 5. Moreover, the TEM images verify the synthesis of spherical and oval-like nanoparticles with even distribution and an average size of approximately 36 nm. Fig. 6 illustrates the EDS microanalysis of the obtained *SPE*-AgNPs. A strong Ag absorption peak appeared at 3 KeV. The Ag, O, and C elements in the chemical composition of *SPE*-AgNPs were detected. These results are directly related to XRD results.

3.5. Particle size distribution and zeta potential measurement

The average diameter of total particles and stability of green synthesized *SPE*-AgNPs were determined by dynamic light scattering (DLS) and zeta potential measurements, as shown

Table 2 MIC and MBC values (μg/ml) for *SPE*-AgNPs tested against Gram-positive and Gram-negative bacteria.

Microorganism	*SPE*-AgNPs		Extract		Ceftriaxone	
	MIC (μg/ml)	MBC (μg/ml)	MIC (mg/ml)	MBC (mg/ml)	MIC (μg/ml)	MBC (μg/ml)
P. aeruginosa ATCC7853	0.78	12.5	50	> 100	3.9	31.25
K. pneumoniae ATCC9997	0.78	1.56	> 100	> 100	1.95	15.62
E. coliATCC25922	0.39	0.39	50	> 100	3.9	15.62
S. epidermidisATCC12228	6.25	200	50	> 100	7.81	62.5
E. faecalis ATCC15753	1.56	200	> 100	> 100	15.62	125
S. aureus ATCC16538	6.25	200	50	> 100	7.81	31.25

in Fig. 7. The negative charges of the products play a key role in the agglomeration formation and thus increase the stability of the products (Rajkumar et al., 2021). The average particle size of the colloidal nanoparticles produced with the aqueous extract of *S. pachycarpa* extract was reported as 107–150 nm. Furthermore, the result of zeta potential reports high stability (due to electrostatic repulsion) of nanoparticles equal to −12.38 mV. The results obtained from the DLS analysis confirm that *SPE*-AgNPs has an adequate surface charge for electrostatic stability to prevent aggregation.

3.6. Analysis of antibacterial and antifungal activities

In this study, the MIC assay was used to evaluate the antibacterial and antifungal activities of synthesized silver nanoparticles using *S. pachycarpa* extract against Gram-positive bacteria (three strains), Gram-negative bacteria (three strains), and *C. albicans* fungi. The results for the synthesized nanoparticles, the antibiotic ceftriaxone, and the antifungal amphotericin B are given in Table. 2. According to the results, silver nanoparticles had an antibacterial effect on all bacterial strains, so that the lowest inhibitory concentration was observed for *E. coli* (MIC value of 0.39 µg/ml) and the highest for *S. epidermidis* and *S. aureus* (MIC values of 6.25 µg/ml). In addition, the broad-spectrum antibiotic ceftriaxone had the most significant effect on *K. pneumoniae* (MIC value of 1.95 µg/ml) and the most minor effect on *E. faecalis* (MIC = 15.62 µg/ ml). Comparison of the results for MIC and MBC in strains showed that the effect of silver nanoparticles on Gram-negative bacteria is more significant than on Gram-positive ones (Fig. 8). The effect of nanoparticles varies in bacterial strains; such variations can be due to the structure, and chemical composition of the cell wall and the mechanisms affecting the activity of various microorganisms studied (Ravichandran et al., 2019). However, the mechanism of antibacterial effect of silver nanoparticles is still unknown. Morones *et al*. showed that silver nanoparticles penetrate bacterial and fungal cells, interact with sulfur and phosphorus-containing compounds such as DNA and ultimately destroy microbes (Morones et al., 2005). The results of the present study showed the antifungal activity of biogenic silver nanoparticles against fungi studied (Table. 3). This nanoparticle even appeared to be superior to amphotericin B, as it had the lowest MIC (0.78 µg/ml) compared to amphotericin B (4 µg/ml). The comparison of the MIC and MBC in bacterial strains also indicated that silver nanoparticles synthesized with *S. pachycarpa* extract had a more substantial antimicrobial effect than the extract alone. The resulting silver nanoparticles not only exhibited promising antimicrobial effects, but also outperformed the broad-spectrum antibiotic ceftriaxone, albeit at lower concentrations. Bacterial resistance has become a severe problem due to improper and widespread use of antibiotics for prevention or therapeutic purposes regardless of actual medical symptoms (García et al., 2020). As a result, nanoparticles seem to be promising alternatives to antibiotics due to their unique properties in combating bacteria (Rajeshkumar et al., 2019).

3.7. Antioxidant activity

In recent years, a variety of methods have been reported to investigate antioxidant activity, one of the most significant of which is DPPH. The DPPH method was used to evaluate the antioxidant properties of the synthesized silver nanoparticles. The DPPH radical is purple when dissolved in an organic

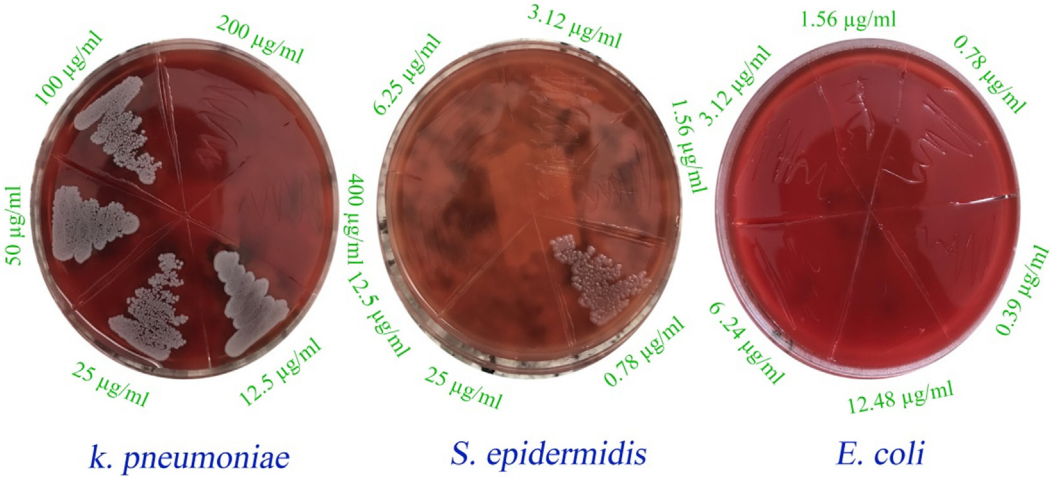

Fig. 8 Photograph of MBC experiments of various bacteria.

Table 3 MIC and MFC of *SPE*-AgNPs and antifungal amphotericin B on *C. albicans*.

Fungal strain	*SPE*-AgNPs		Extract		Amphotericin B	
	MIC (µg/ml)	MFC (µg/ml)	MIC (mg/ml)	MFC (mg/ml)	MIC (µg/ml)	MFC (µg/ml)
C. albicans	0.78	0.78	> 100	25	4	8

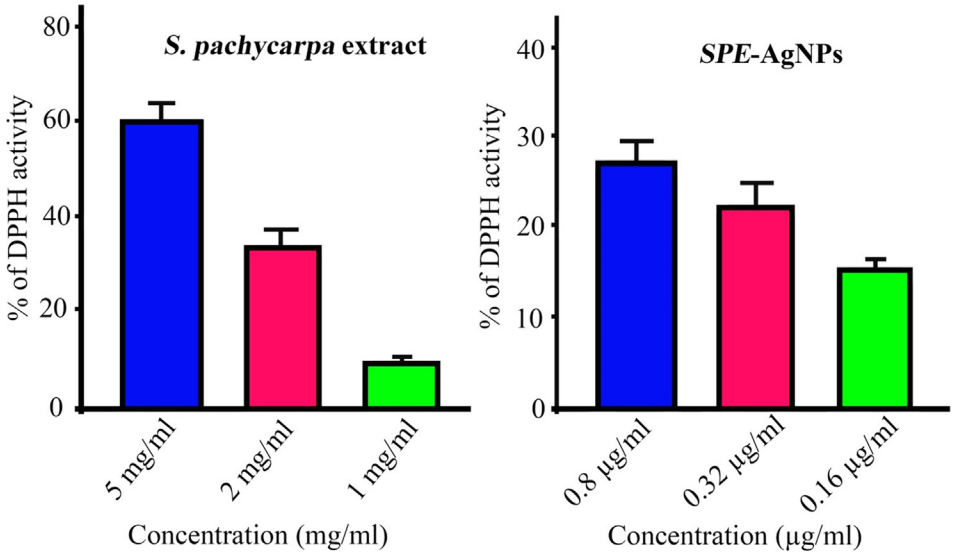

Fig. 9 DPPH inhibition percentage at different concentrations of *SPE*-AgNPs.

solvent, while turns yellow when exposed to a reducing agent or a hydrogen donor. Such a change can be measured at the wavelength of 517 nm. Chemical and biological compounds with regenerative properties can neutralize such radicals, and the decrease in color intensity at the wavelength of 517 nm indicates stronger neutralizing effect. In this research, the percentage of inhibition of DPPH by *S. pachycarpa* extract and *SPE*-AgNPs were studied in three concentrations. Our results showed that silver nanoparticles at a concentration of 0.16 µg/ml had an antioxidant effect 15.5% and that higher concentrations led to a more substantial antioxidant property (Fig. 9). Comparing the antioxidant effect in the two groups of silver nanoparticles and *S. pachycarpa* extract showed that synthesized silver nanoparticles using extract had a better antioxidant effect at much lower concentrations than the pure extract. However, the current research is similar to findings that have emerged from Jalilian *et al.* (Jalilian et al., 2020).

3.8. Antitumor effects on K562 cells

To assess the toxic effects of *SPE*-AgNPs on the K562 cell line, MTT colorimetry was used. For this purpose, 20,000 cells were cultured in each micro-well and treated with different concentrations of the medication for 24 h. The results confirmed the antitumor effect on reducing the cell growth compared to the control group. The results also showed that such an effect had a significant association with the concentration, so that within 24 h of treatment at a concentration of 50 µg/ml, the highest decrease in cell growth was observed (97%). The IC50 value of the medication was determined (IC50 of 19.5 µg/ml Calcusyn software was used). Our cytostatic results demonstrated *SPE*-AgNPs decreased viability of K562 cells in a dose-dependent manner (Fig. 10). Similarly, a 2014 study by Mousavi on the apoptotic features and cytotoxicity of *S. pachycarpa* showed significant toxicity against the HeLa, HL-60, MCF-7, A549, and PC3 cell lines (Mousavi et al., 2014).

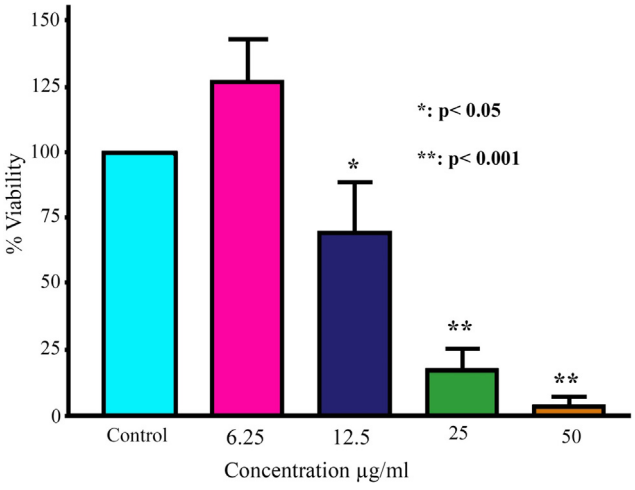

Fig. 10 Cytotoxic effect of *SPE*-AgNPs (sample no. 11) against K562 cancer cell line.

3.9. Photocatalytic properties

The synthesized nano-scale AgNPs using *S. pachycarpa* extract as capping, stabilizing, and reducing agents were used as UV and sun-light responsive photocatalytic to degrade the methylene blue and eriochrome black T pollutants as common organic pollutant released from industrial wastewater. The photocatalytic performance of all the samples at various time intervals of irradiations was studied. As expected, no degradation has occurred without the usage of *SPE*-AgNPs as a nanocatalyst. The photocatalytic results showed that the photo-degradation of EBT and MB contaminants was 96.23% and 90.06% under UV irradiation and 84.57% and 79.18% under sunlight irradiation after 80 min (Fig. 11). High uniformity, small size, and good surface area can be reasons for superior action of biogenic silver nanoparticles (*SPE*-

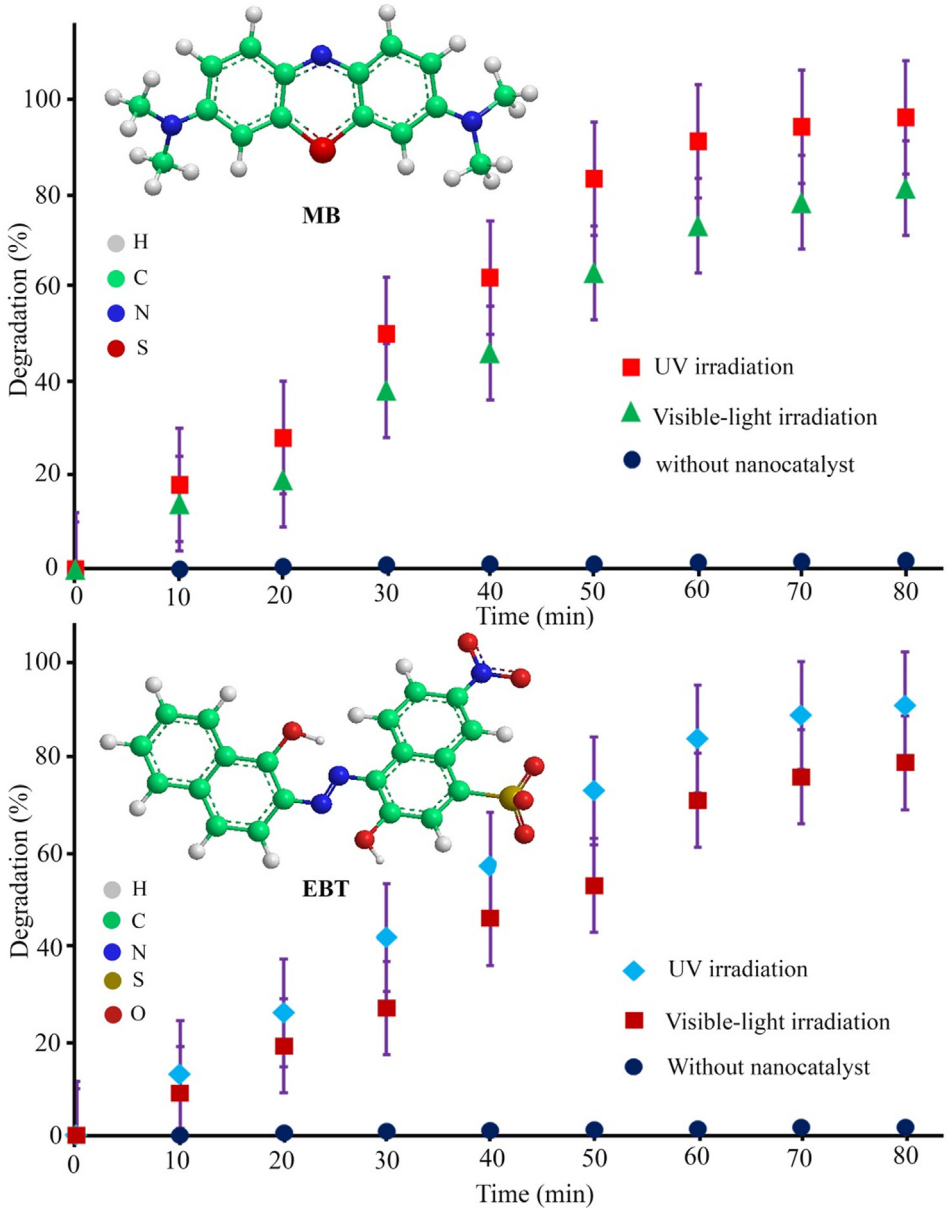

Fig. 11 Photocatalytic degradation of EBT and MB organic dyes by optimal *SPE*-AgNPs (40 mM, 60 min and 85 °C).

AgNPs) in dyes degradation under sun-light and UV irradiations (Zinatloo-Ajabshir et al., 2019). Upon closer examination of the results, we conclude that the photodegradation of methylene blue as a cationic pollutant is higher than eriochrome black T as an anionic pollutants. This increase could be due oxygen group and positive charge in the molecular structure of cationic contaminant. The possible mechanism of degradation of cationic and anionic pollutants using synthesized silver nanoparticles can be displayed as follows (Scheme.1):

$$SPE - \mathrm{AgNPs} + h\nu \rightarrow SPE - \mathrm{AgNPs}(e^{-}_{CB} + h^{+}_{VB}) \quad (5)$$

$$SPE\text{-AgNPs}\ (h_{uv}) + H_2O \rightarrow Ag^0 + H + OH \quad (6)$$

$$O_2^{\cdot-} + H^+ \rightarrow HO_2^{\cdot} \quad (7)$$

$$\mathrm{Dye} + OH^{\cdot} \rightarrow \mathrm{degradationsamples} \quad (8)$$

$$\mathrm{Dye} + h^{+}_{VB} \rightarrow \mathrm{oxidationsamples} \quad (9)$$

$$\mathrm{Dye} + e^{-}_{CB} \rightarrow \mathrm{reductionsamples} \quad (10)$$

4. Conclusion

Spherical and oval-like silver nanoparticles with an average size of 30–40 nm were synthesized using *S. pachycarpa* extract. XRD pattern showed that the *SPE*-AgNPs were in the face-centered cubic (fcc) structure. FTIR spectra confirmed the capping behavior of the *S. pachycarpa* extract. The synthesized *SPE*-AgNPs exhibited high antibacterial, antioxidant, anticancer and catalytic activities. *SPE*-AgNPs demonstrated stronger antibacterial and antifungal activities than ceftriaxone and amphotericin B, respectively. High anticancer activity of *SPE*-AgNPs was obtained on K562 cancer cells with the

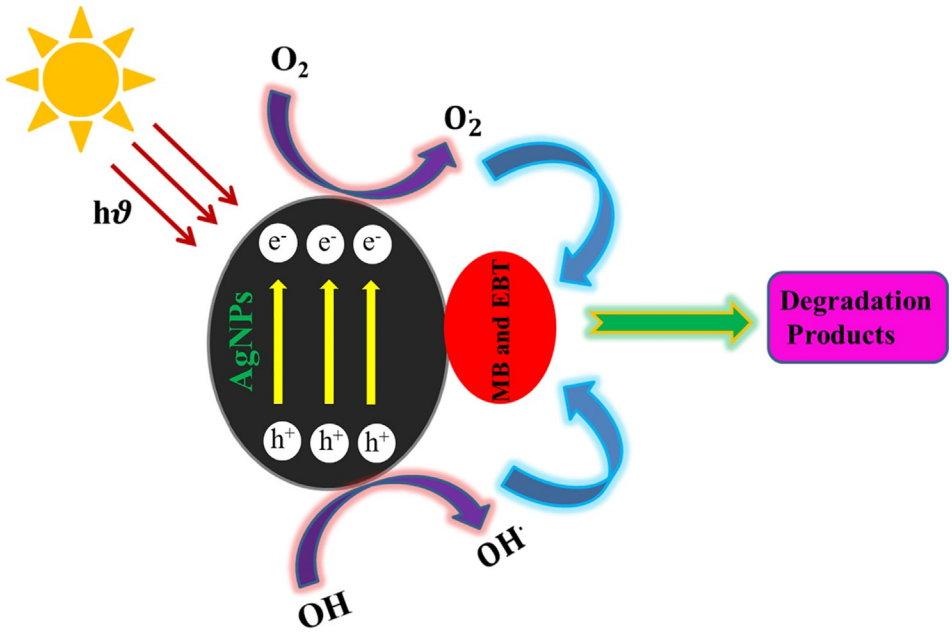

Scheme 1 Mechanism of photocatalytic degradation of organic dyes by *SPE*-AgNPs.

IC50 value of 19.5 μg/ml. Furthermore, the results showed that the *SPE*-AgNPs as a nanocatalyst had excellent photocatalytic activity for degradation of EBT and MB under sun-light and UV irradiations. This study suggests that *SPE*-AgNPs can be effective nanoparticles for environmental and biological applications.

Declaration of Competing Interest

The authors declare that they have no known competing financial interests or personal relationships that could have appeared to influence the work reported in this paper.

Acknowledgment

In this investigation, the entire procedures were conducted according to the Helsinki Declaration and ethical standards of the institutional research committee. The ethics code was taken from Birjand University of Medical Sciences (IR.BUMS.REC.1399.126).

References

Ahmadi, S., Fazilati, M., Mousavi, S.M., Nazem, H., 2020a. Antibacterial/fungal and anti-cancer performance of green synthesized Ag nanoparticles using summer savory extract. J. Exp. Nanosci. 15 (1), 363–380.

Ahmadi, S., Rahdar, A., Igwegbe, C.A., Mortazavi-Derazkola, S., Banach, A.M., Rahdar, S., Singh, A.K., Rodriguez-Couto, S., Kyzas, G.Z., 2020b. Praseodymium-doped cadmium tungstate ($CdWO_4$) nanoparticles for dye degradation with sonocatalytic process. Polyhedron 190, 114792.

Ahmed, M.J., Murtaza, G., Rashid, F., Iqbal, J., 2019. Eco-friendly green synthesis of silver nanoparticles and their potential applications as antioxidant and anticancer agents. Drug Dev. Ind. Pharm. 45 (10), 1682–1694.

Anandan, M., Poorani, G., Boomi, P., Varunkumar, K., Anand, K., Chuturgoon, A.A., Saravanan, M., H., 2019. Gurumallesh Prabu, Green synthesis of anisotropic silver nanoparticles from the aqueous leaf extract of Dodonaea viscosa with their antibacterial and anticancer activities. Process Biochem. 80, 80–88.

Ardestani, M.S., Bitarafan-Rajabi, A., Mohammadzadeh, P., Mortazavi-Derazkola, S., Sabzevari, O., Azar, A.D., Kazemi, S., Hosseini, S.R., Ghoreishi, S.M., 2020. Synthesis and characterization of novel 99mTc-DGC nano-complexes for improvement of heart diagnostic. Bioorg. Chem. 96, 103572.

Awwad, A.M., Salem, N.M., Abdeen, A.O., 2013. Green synthesis of silver nanoparticles using carob leaf extract and its antibacterial activity. Int. J. Ind. Chem. 4 (1), 29.

Azeez, F., Al-Hetlani, E., Arafa, M., Abdelmonem, Y., Nazeer, A.A., Amin, M.O., Madkour, M., 2018. The effect of surface charge on photocatalytic degradation of methylene blue dye using chargeable titania nanoparticles. Sci. Rep. 8 (1), 7104.

Beyene, H.D., Werkneh, A.A., Bezabh, H.K., Ambaye, T.G., 2017. Synthesis paradigm and applications of silver nanoparticles (AgNPs), a review, Sustainable. Mater. Technol. 13, 18–23.

Chandra, H., Kumari, P., Bontempi, E., Yadav, S., 2020. Medicinal plants: Treasure trove for green synthesis of metallic nanoparticles and their biomedical applications. Biocatal. Agric. Biotechnol. 24, 101518.

Ebrahimzadeh, M.A., Mortazavi-Derazkola, S., Zazouli, M.A., 2019. Eco-friendly green synthesis and characterization of novel Fe_3O_4/SiO_2/Cu_2O–Ag nanocomposites using Crataegus pentagyna fruit extract for photocatalytic degradation of organic contaminants. J. Mater. Sci.: Mater. Electron. 30 (12), 10994–11004.

Ebrahimzadeh, M.A., Naghizadeh, A., Mohammadi-Aghdam, S., Khojasteh, H., Ghoreishi, S.M., Mortazavi-Derazkola, S., 2020a. Enhanced catalytic and antibacterial efficiency of biosynthesized Convolvulus fruticosus extract capped gold nanoparticles (CFE@AuNPs). J. Photochem. Photobiol., B 209, 111949.

Ebrahimzadeh, M.A., Mortazavi-Derazkola, S., Zazouli, M.A., 2020b. Eco-friendly green synthesis of novel magnetic Fe_3O_4/SiO_2/ZnO-Pr_6O_{11} nanocomposites for photocatalytic degradation of organic pollutant. J. Rare Earths 38 (1), 13–20.

Emami, S.A., Amin-Ar-Ramimeh, E., Ahi, A., Bolourian Kashy, M. R., Schneider, B., Iranshahi, M., 2007. Prenylated Flavonoids and Flavonostilbenes from Sophora pachycarpa. Roots. Pharm. Biol. 45 (6), 453–457.

Fouda, A., Hassan, S.-E.-D., Abdo, A.M., El-Gamal, M.S., 2020. Antimicrobial, Antioxidant and Larvicidal Activities of Spherical Silver Nanoparticles Synthesized by Endophytic Streptomyces spp. Biol. Trace Elem. Res. 195 (2), 707–724.

García, J., García-Galán, M.J., Day, J.W., Boopathy, R., White, J.R., Wallace, S., Hunter, R.G., 2020. A review of emerging organic contaminants (EOCs), antibiotic resistant bacteria (ARB), and antibiotic resistance genes (ARGs) in the environment: Increasing removal with wetlands and reducing environmental impacts. Bioresour. Technol. 307, 123228.

Garibo, D., Borbón-Nuñez, H.A., de León, J.N.D., García Mendoza, E., Estrada, I., Toledano-Magaña, Y., Tiznado, H., Ovalle-Marroquin, M., Soto-Ramos, A.G., Blanco, A., Rodríguez, J.A., Romo, O.A., Chávez-Almazán, L.A., Susarrey-Arce, A., 2020. Green synthesis of silver nanoparticles using Lysiloma acapulcensis exhibit high-antimicrobial activity. Sci. Rep. 10 (1), 12805.

Ghoreishi, S.M., 2017. Facile synthesis and characterization of $CaWO_4$ nanoparticles using a new Schiff base as capping agent: enhanced photocatalytic degradation of methyl orange. J. Mater. Sci.: Mater. Electron. 28 (19), 14833–14838.

Ghoreishi, S.M., Khalaj, A., Bitarafan-Rajabi, A., Azar, A.D., Ardestani, M.S., Assadi, A., 2017. Novel 99mTc-Radiolabeled Anionic Linear Globular PEG-Based Dendrimer-Chlorambucil: Non-Invasive Method for In-Vivo Biodistribution. Drug Res. 67 (3), 149–155.

Guo, H., Fan, S., Liu, J., Wang, Y., 2021. Facile synthesis of superparamagnetic manganese ferrite nanoparticles as a novel T2 MRI contrast agent. J. Indian Chem. Soc. 98, (10) 100163.

Hashemi, S.F., Tasharrofi, N., Saber, M.M., 2020. Green synthesis of silver nanoparticles using Teucrium polium leaf extract and assessment of their antitumor effects against MNK45 human gastric cancer cell line. J. Mol. Struct. 1208, 127889.

Hebeish, A., El-Rafie, M.H., El-Sheikh, M.A., El-Naggar, M.E., 2013. Nanostructural Features of Silver Nanoparticles Powder Synthesized through Concurrent Formation of the Nanosized Particles of Both Starch and Silver. J. Nanotechnol. 2013, 201057.

Iravani, S., Korbekandi, H., Mirmohammadi, S.V., Zolfaghari, B., 2014. Synthesis of silver nanoparticles: chemical, physical and biological methods. Res. Pharm. Sci. 9 (6), 385–406.

Jalilian, F., Chahardoli, A., Sadrjavadi, K., Fattahi, A., Shokoohinia, Y., 2020. Green synthesized silver nanoparticle from Allium ampeloprasum aqueous extract: Characterization, antioxidant activities, antibacterial and cytotoxicity effects. Adv. Powder Technol. 31 (3), 1323–1332.

Jorge de Souza, T.A., Rosa Souza, L.R., Franchi, L.P., 2019. Silver nanoparticles: An integrated view of green synthesis methods, transformation in the environment, and toxicity. Ecotoxicol. Environ. Saf. 171, 691–700.

Judith Vijaya, J., Jayaprakash, N., Kombaiah, K., Kaviyarasu, K., John Kennedy, L., Jothi Ramalingam, R., Al-Lohedan, H.A., V. M, M.-A., Maaza, M., 2017. Bioreduction potentials of dried root of Zingiber officinale for a simple green synthesis of silver nanoparticles: Antibacterial studies. J. Photochem. Photobiol. B: Biol. 177, 62–68.

Kadam, J., Dhawal, P., Barve, S., Kakodkar, S., 2020. Green synthesis of silver nanoparticles using cauliflower waste and their multi-faceted applications in photocatalytic degradation of methylene blue dye and Hg2+ biosensing. SN Appl. Sci. 2 (4), 738.

Klein, E., Vánky, F., Ben-Bassat, H., Neumann, H., Ralph, P., Zeuthen, J., Polliack, A., 1976. Properties of the K562 cell line, derived from a patient with chronic myeloid leukemia. Int. J. Cancer 18 (4), 421–431.

Kumar, S., Pandey, A.K., 2013. Chemistry and Biological Activities of Flavonoids: An Overview. Sci. World J. 2013, 162750.

Li, S., Al-Misned, F.A., El-Serehy, H.A., Yang, L., 2021. Green synthesis of gold nanoparticles using aqueous extract of Mentha Longifolia leaf and investigation of its anti-human breast carcinoma properties in the in vitro condition. Arabian J. Chem. 14, (2) 102931.

Mekasuwandumrong, O., Pawinrat, P., Praserthdam, P., Panpranot, J., 2010. Effects of synthesis conditions and annealing post-treatment on the photocatalytic activities of ZnO nanoparticles in the degradation of methylene blue dye. Chem. Eng. J. 164 (1), 77–84.

Mohammadi-Aghdam, S., Valinezhad-Saghezi, B., Mortazavi, Y., Qhoreishi, S.M., 2018. Modified Fe_3O_4/HAP magnetically nanoparticles as the carrier for ibuprofen: Adsorption and release study. Drug Res. 69 (2), 93–99.

Mohammadzadeh, P., Cohan, R.A., Ghoreishi, S.M., Bitarafan-Rajabi, A., Ardestani, M.S., 2017. AS1411 Aptamer-Anionic Linear Globular Dendrimer G2-Iohexol Selective Nano-Theranostics. Sci. Rep. 7 (1), 11832.

Mohammadzadeh, P., Ardestani, M.S., Mortazavi-Derazkola, S., Bitarafan-Rajabi, A., Ghoreishi, S.M., 2019. PEG-Citrate dendrimer second generation: Is this a good carrier for imaging agents in vitro and in vivo? IET Nanobiotechnol. 13 (6), 560–564.

Morabbi Najafabad, A., Jamei, R., 2014. Free radical scavenging capacity and antioxidant activity of methanolic and ethanolic extracts of plum (Prunus domestica L.) in both fresh and dried samples. Avicenna J. Phytomed. 4 (5), 343–353.

Morones, J.R., Elechiguerra, J.L., Camacho, A., Holt, K., Kouri, J.B., Ramírez, J.T., Yacaman, M.J., 2005. The bactericidal effect of silver nanoparticles. Nanotechnology 16 (10), 2346–2353.

Mosmann, T., 1983. Rapid colorimetric assay for cellular growth and survival: Application to proliferation and cytotoxicity assays. J. Immunol. Methods 65 (1), 55–63.

Mousavi, S.H., Motaez, M., Zamiri-Akhlaghi, A., Emami, S.A., Tayarani-Najaran, Z., 2014. In-vitro Evaluation of Cytotoxic and Apoptogenic Properties of Sophora Pachycarpa. Iran J. Pharm. Res. 13 (2), 665–673.

Naghizadeh, A., Mizwari, Z.M., Ghoreishi, S.M., Lashgari, S., Mortazavi-Derazkola, S., Rezaie, B., 2021. Biogenic and eco-benign synthesis of silver nanoparticles using jujube core extract and its performance in catalytic and pharmaceutical applications: Removal of industrial contaminants and in-vitro antibacterial and anticancer activities. Environ. Technol. Innovation 23, 101560.

Rafique, M., Sadaf, I., Rafique, M.S., Tahir, M.B., 2017. A review on green synthesis of silver nanoparticles and their applications. Artif. Cells Nanomed. Biotechnol. 45 (7), 1272–1291.

Rajeshkumar, S., Bharath, L.V., Geetha, R., 2019. Chapter 17 - Broad spectrum antibacterial silver nanoparticle green synthesis: Characterization, and mechanism of action. In: Shukla, A.K., Iravani, S. (Eds.), Green Synthesis, Characterization and Applications of Nanoparticles. Elsevier, pp. 429–444.

Rajkumar, R., Ezhumalai, G., Gnanadesigan, M., 2021. A green approach for the synthesis of silver nanoparticles by Chlorella vulgaris and its application in photocatalytic dye degradation activity. Environ. Technol. Innovation 21, 101282.

Rao, C.R.K., Trivedi, D.C., 2006. Biphasic synthesis of fatty acids stabilized silver nanoparticles: Role of experimental conditions on particle size. Mater. Chem. Phys. 99 (2), 354–360.

Ravichandran, V., Vasanthi, S., Shalini, S., Shah, S.A.A., Tripathy, M., Paliwal, N., 2019. Green synthesis, characterization, antibacterial, antioxidant and photocatalytic activity of Parkia speciosa leaves extract mediated silver nanoparticles. Results Phys. 15, 102565.

Riesenberg, A., Kaspar, H., Feßler, A.T., Werckenthin, C., Schwarz, S., 2016. Susceptibility testing of Rhodococcus equi: An interlaboratory test. Vet. Microbiol. 194, 30–35.

Shirzadi-Ahodashti, M., Ebrahimzadeh, M.A., Ghoreishi, S.M., Naghizadeh, A., Mortazavi-Derazkola, S., 2020a. Facile and eco-benign synthesis of a novel $MnFe_2O_4$@SiO_2@Au magnetic

nanocomposite with antibacterial properties and enhanced photocatalytic activity under UV and visible-light irradiations. Appl. Organomet. Chem. 34, (5) e5614.

Shirzadi-Ahodashti, M., Mortazavi-Derazkola, S., Ebrahimzadeh, M. A., 2020b. Biosynthesis of noble metal nanoparticles using crataegus monogyna leaf extract (CML@X-NPs, X = Ag, Au): Antibacterial and cytotoxic activities against breast and gastric cancer cell lines. Surf. Interfaces 21, 100697.

Shirzadi-Ahodashti, M., Mizwari, Z.M., Hashemi, Z., Rajabalipour, S., Ghoreishi, S.M., Mortazavi-Derazkola, S., Ebrahimzadeh, M. A., 2021a. Discovery of high antibacterial and catalytic activities of biosynthesized silver nanoparticles using C. fruticosus (CF-AgNPs) against multi-drug resistant clinical strains and hazardous pollutants. Environ. Technol. Innovation 23, 101607.

Shirzadi-Ahodashti, M., Hashemi, Z., Mortazavi, Y., Khormali, K., Mortazavi-Derazkola, S., Ebrahimzadeh, M.A., 2021b. Discovery of high antibacterial and catalytic activities against multi-drug resistant clinical bacteria and hazardous pollutants by biosynthesized of silver nanoparticles using Stachys inflata extract (AgNPs@SI). Colloids Surf., A 617, 126383.

Yoo, B., Ma, K., Zhang, L., Burns, A., Sequeira, S., Mellinghoff, I., Brennan, C., Wiesner, U., Bradbury, M.S., 2015. Ultrasmall dual-modality silica nanoparticle drug conjugates: Design, synthesis, and characterization. Bioorg. Med. Chem. 23 (22), 7119–7130.

Zinatloo-Ajabshir, S., Morassaei, M.S., Salavati-Niasari, M., 2019. Facile synthesis of $Nd_2Sn_2O_7$-SnO_2 nanostructures by novel and environment-friendly approach for the photodegradation and removal of organic pollutants in water. J. Environ. Manage. 233, 107–119.